geopress

Modeling the Ionosphere-Thermosphere System

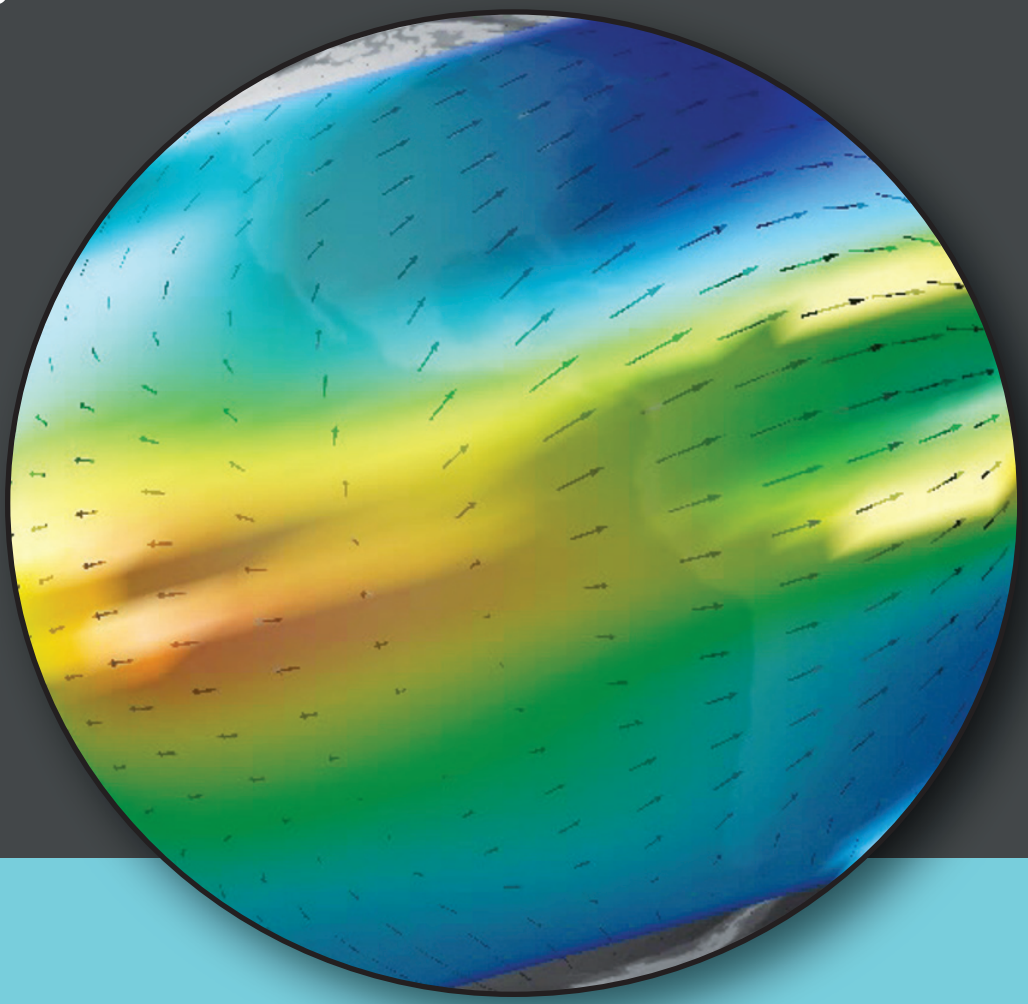

J.D. Huba, R.W. Schunk, and G.V. Khazanov
Editors

AGU
American Geophysical Union

Geophysical Monograph Series

Including
IUGG Volumes
Maurice Ewing Volumes
Mineral Physics Volumes

166 **Back-Arc Spreading Systems: Geological, Biological, Chemical, and Physical Interactions** *David M. Christie, Charles Fisher, Sang-Mook Lee, and Sharon Givens (Eds.)*

167 **Recurrent Magnetic Storms: Corotating Solar Wind Streams** *Bruce Tsurutani, Robert McPherron, Walter Gonzalez, Gang Lu, José H. A. Sobral, and Natchimuthukonar Gopalswamy (Eds.)*

168 **Earth's Deep Water Cycle** *Steven D. Jacobsen and Suzan van der Lee (Eds.)*

169 **Magnetospheric ULF Waves: Synthesis and New Directions** *Kazue Takahashi, Peter J. Chi, Richard E. Denton, and Robert L. Lysak (Eds.)*

170 **Earthquakes: Radiated Energy and the Physics of Faulting** *Rachel Abercrombie, Art McGarr, Hiroo Kanamori, and Giulio Di Toro (Eds.)*

171 **Subsurface Hydrology: Data Integration for Properties and Processes** *David W. Hyndman, Frederick D. Day-Lewis, and Kamini Singha (Eds.)*

172 **Volcanism and Subduction: The Kamchatka Region** *John Eichelberger, Evgenii Gordeev, Minoru Kasahara, Pavel Izbekov, and Johnathan Lees (Eds.)*

173 **Ocean Circulation: Mechanisms and Impacts—Past and Future Changes of Meridional Overturning** *Andreas Schmittner, John C. H. Chiang, and Sidney R. Hemming (Eds.)*

174 **Post-Perovskite: The Last Mantle Phase Transition** *Kei Hirose, John Brodholt, Thorne Lay, and David Yuen (Eds.)*

175 **A Continental Plate Boundary: Tectonics at South Island, New Zealand** *David Okaya, Tim Stem, and Fred Davey (Eds.)*

176 **Exploring Venus as a Terrestrial Planet** *Larry W. Esposito, Ellen R. Stofan, and Thomas E. Cravens (Eds.)*

177 **Ocean Modeling in an Eddying Regime** *Matthew Hecht and Hiroyasu Hasumi (Eds.)*

178 **Magma to Microbe: Modeling Hydrothermal Processes at Oceanic Spreading Centers** *Robert P. Lowell, Jeffrey S. Seewald, Anna Metaxas, and Michael R. Perfit (Eds.)*

179 **Active Tectonics and Seismic Potential of Alaska** *Jeffrey T. Freymueller, Peter J. Haeussler, Robert L. Wesson, and Göran Ekström (Eds.)*

180 **Arctic Sea Ice Decline: Observations, Projections, Mechanisms, and Implications** *Eric T. DeWeaver, Cecilia M. Bitz, and L.-Bruno Tremblay (Eds.)*

181 **Midlatitude Ionospheric Dynamics and Disturbances** *Paul M. Kintner, Jr., Anthea J. Coster, Tim Fuller-Rowell, Anthony J. Mannucci, Michael Mendillo, and Roderick Heelis (Eds.)*

182 **The Stromboli Volcano: An Integrated Study of the 2002–2003 Eruption** *Sonia Calvari, Salvatore Inguaggiato, Giuseppe Puglisi, Maurizio Ripepe, and Mauro Rosi (Eds.)*

183 **Carbon Sequestration and Its Role in the Global Carbon Cycle** *Brian J. McPherson and Eric T. Sundquist (Eds.)*

184 **Carbon Cycling in Northern Peatlands** *Andrew J. Baird, Lisa R. Belyea, Xavier Comas, A. S. Reeve, and Lee D. Slater (Eds.)*

185 **Indian Ocean Biogeochemical Processes and Ecological Variability** *Jerry D. Wiggert, Raleigh R. Hood, S. Wajih A. Naqvi, Kenneth H. Brink, and Sharon L. Smith (Eds.)*

186 **Amazonia and Global Change** *Michael Keller, Mercedes Bustamante, John Gash, and Pedro Silva Dias (Eds.)*

187 **Surface Ocean–Lower Atmosphere Processes** *Corinne Le Quèrè and Eric S. Saltzman (Eds.)*

188 **Diversity of Hydrothermal Systems on Slow Spreading Ocean Ridges** *Peter A. Rona, Colin W. Devey, Jérôme Dyment, and Bramley J. Murton (Eds.)*

189 **Climate Dynamics: Why Does Climate Vary?** *De-Zheng Sun and Frank Bryan (Eds.)*

190 **The Stratosphere: Dynamics, Transport, and Chemistry** *L. M. Polvani, A. H. Sobel, and D. W. Waugh (Eds.)*

191 **Rainfall: State of the Science** *Firat Y. Testik and Mekonnen Gebremichael (Eds.)*

192 **Antarctic Subglacial Aquatic Environments** *Martin J. Siegert, Mahlon C. Kennicut II, and Robert A. Bindschadler*

193 **Abrupt Climate Change: Mechanisms, Patterns, and Impacts** *Harunur Rashid, Leonid Polyak, and Ellen Mosley-Thompson (Eds.)*

194 **Stream Restoration in Dynamic Fluvial Systems: Scientific Approaches, Analyses, and Tools** *Andrew Simon, Sean J. Bennett, and Janine M. Castro (Eds.)*

195 **Monitoring and Modeling the *Deepwater Horizon* Oil Spill: A Record-Breaking Enterprise** *Yonggang Liu, Amy MacFadyen, Zhen-Gang Ji, and Robert H. Weisberg (Eds.)*

196 **Extreme Events and Natural Hazards: The Complexity Perspective** *A. Surjalal Sharma, Armin Bunde, Vijay P. Dimri, and Daniel N. Baker (Eds.)*

197 **Auroral Phenomenology and Magnetospheric Processes: Earth and Other Planets** *Andreas Keiling, Eric Donovan, Fran Bagenal, and Tomas Karlsson (Eds.)*

198 **Climates, Landscapes, and Civilizations** *Liviu Giosan, Dorian Q. Fuller, Kathleen Nicoll, Rowan K. Flad, and Peter D. Clift (Eds.)*

199 **Dynamics of the Earth's Radiation Belts and Inner Magnetosphere** *Danny Summers, Ian R. Mann, Daniel N. Baker, and Michael Schulz (Eds.)*

200 **Langrangian Modeling of the Atmosphere** *John Lin, Dominik Brunner, Christopher Gerbig, Andreas Stohl, Ashok Luhar, Peter Webley*

geopress

Geophysical Monograph 201

Modeling the Ionosphere–Thermosphere System

Joseph Huba
Robert Schunk
George Khazanov
Editors

American Geophysical Union
Washington, DC

Published under the aegis of the AGU Books Board

Kenneth R. Minschwaner, Chair; Gray E. Bebout, Kenneth H. Brink, Jiasong Fang, Ralf R. Haese, Yonggang Liu, W. Berry Lyons, Laurent Montési, Nancy N. Rabalais, Todd C. Rasmussen, A. Surjalal Sharma, David E. Siskind, Rigobert Tibi, and Peter E. van Keken, members.

Library of Congress Cataloging-in-Publication Data

Modeling the ionosphere-thermosphere system / Joseph Huba, Robert Schunk, George Khazanov, editors.
pages cm.—(Geophysical monograph, ISSN 0065-8448 ; 201)
Includes bibliographical references and index.

ISBN 978-0-87590-491-7

1. Ionosphere–Mathematical models. 2. Thermosphere–Mathematical models. 3. Atmospheric thermodynamics. 4. Dynamic meteorology. I. Huba, J. D. (Joseph D.), 1950– editor of compilation. II. Schunk, R. W. (Robert W.), editor of compilation. III. Khazanov, G. V. (Georgii Vladimirovich), editor of compilation.

QC881.2.I6M62 2014

551.51–dc23

2013050020

ISBN: 978-0-87590-490-0
ISSN: 0065-8448

Cover Image: Ash plume from Augustine Volcano on 30 January 2006 during its eruptive stage. Photograph of the plume at 13:09 AKST (22:09 UTC). Photograph credit: Game McGimsey. Image courtesy of Alaska Volcano Observatory/United States Geological Survey. (inset) PUFF volcanic ash Lagrangian Dispersion Particle Model (LDPM) at 22:09 UTC with ash particles indicated by altitude above sea level. Graph courtesy of Peter Webley, Geophysical Institute, University of Alaska Fairbanks.

Printed in the United States of America.

CONTENTS

Section IV: Validation of IT Models

Section V: IT Coupling: Above and Below

Section VI: Equatorial Ionospheric Processes

Section VII: Data Assimilation

Section VIII: Applications

PREFACE

The importance of large-scale numerical models to understand the complex dynamics of the ionosphere/thermosphere (IT) system has been recognized for over three decades. Many ionosphere and thermosphere models have been developed, both as separate and coupled models; they have been used to investigate IT dynamics and compare model results to observational data. However, until a few years ago, there have been very few (if any) conference sessions or workshops devoted solely to the development and understanding of computational IT models.

To address this problem, a session on ionosphere/thermosphere modeling was organized by myself, Aaron Ridley, and Bob Schunk at the 2009 NSF CEDAR workshop held in Santa Fe, New Mexico. The session description was as follows:

> The workshop will focus on IT modeling of the low solar activity (solar minimum or quiet) time, low- to mid-latitude ionosphere. It is hoped that a description of each model will be presented, highlighting (1) basic equations actually solved, (2) numerical techniques, (3) strong and weak points (both physics and numerics), i.e., the good, the bad, and the ugly, and (4) simulation results from a specified day. Results from the different studies can be compared and an ensemble average could be presented and compared to data. Finally, issues that need to be resolved to improve models could be addressed.

The session was extremely successful (i.e., well attended with ample discussion; perhaps, in part, because of a favorable time slot early in the week). Given the enthusiasm for the topic, Bob Schunk suggested we hold a Chapman Conference on IT modeling. I agreed to look into the matter and subsequently submitted a proposal to AGU requesting a Chapman Conference with myself, Bob Schunk, and Aaron Ridley as the conveners. The proposal was accepted, and we held a Chapman Conference on "Modeling the Ionosphere/Thermosphere System" in Charleston, South Carolina, on 9–12 May 2011.

This monograph is an outgrowth of the conference and represents a compilation of different aspects of modeling the IT system. The papers include tutorials on basic ionosphere/thermosphere physics, descriptions of numerical methods and models, and applications to important ionospheric phenomena (e.g., onset and evolution of irregularities) and space weather (e.g., data assimilation). As such, this book serves to provide a basic introduction to IT modeling and to make the IT community aware of the strengths, as well as limitations, of current modeling capabilities and the need for future development.

J.D. Huba
Naval Research Laboratory

Modeling the Ionosphere-Thermosphere System
Geophysical Monograph Series 201

10.1029/2013GM001452

Introduction

The science focus of the monograph is the physics of the coupled ionosphere/thermosphere (IT) system. This system is controlled largely by local ion-neutral processes, but there can be strong forcings from below (e.g., tides, gravity waves, and upper atmosphere winds) and above (e.g., solar EUV, high-latitude heating from precipitating electrons, and region 1 and 2 current systems) that impact its behavior. Thus, it is not an isolated system but can be thought of as a transition layer between the Earth's atmosphere and space; viewed from this vantage point, it is clear that it plays a vital role in forecasting space weather.

Given the complexity of the IT system, large-scale computational models of the ionosphere and thermosphere are required to provide a basic understanding of the key physical processes that govern the system, as well as to provide a quantitative description of its behavior that can be compared to observational data. Such models have been developed and are being used extensively to understand and model the IT system, as well as to aid in the development of space weather operational systems. The objective of the monograph is to provide the IT community with the following: (1) a basic description of IT models including the equations that are solved and the numerical methods and algorithms used, (2) examples of applications to the IT system with comparisons to data, (3) assessment of strengths and weaknesses of the models, (4) test simulations that elucidate those strengths and weaknesses, and (5) identification of future efforts to improve the IT modeling capability.

The monograph is divided into the following sections: (1) Physical Processes and Numerical Methods, (2) Ionosphere/Thermosphere Models, (3) Response From Forcings Below and Above, (4) Ionospheric Irregularities, (5) Data Assimilation Models, (6) Metrics and Validation, and (7) Space Weather and the Future. Each section contains papers that describe the current state of research in these areas, as well as providing insight into future development of models to improve our understanding of the ionosphere/thermosphere system.

J. D. Huba, Naval Research Laboratory, Plasma Physics Division, Code 6790, Washington, DC 20375-5320, USA. (huba@ppd.nrl.navy.mil)

G. V. Khazanov, NASA/GSFC, code 673, 8800 Greenbelt Rd, Greenbelt, MD 20771, USA.

R. W. Schunk, Utah State University, Center for Atmospheric and Space Sciences, Utah State University, 4405 Old Main Hill, Logan, UT 84322-4405, USA.

Modeling the Ionosphere-Thermosphere System
Geophysical Monograph Series 201

10.1029/2013GM001453

Ionosphere-Thermosphere Physics: Current Status and Problems

R. W. Schunk

Center for Atmospheric and Space Sciences, Utah State University, Logan, Utah, USA

The ionosphere-thermosphere (I-T) system is a highly dynamic, nonlinear, and complex medium that varies with altitude, latitude, longitude, time, season, solar cycle, and geomagnetic activity. Despite its complex nature, significant progress has been made during the last three decades in modeling the global I-T system. The climatology of the system has been clearly established, and the global I-T models have been able to reproduce the major I-T features. However, the global I-T models have been less successful in modeling weather features, and even with regard to climatology, there has been limited quantitative success when comparing global I-T models with measurements. The problem with the global models is that they are usually based on simple mathematical formulations, the model resolutions are coarse, the models contain uncertain parameters, the coupling between the I-T models is incomplete, and there is missing physics in all of the global models. Here the focus is on providing examples of the missing physics and how it affects the ionosphere and/or thermosphere.

1. INTRODUCTION

The ionosphere-thermosphere (I-T) system is a highly dynamic and complex medium that varies significantly, and this variation is particularly strong during geomagnetic storms and substorms. The complex nature of the I-T system results primarily from the fact that it is an open and externally driven system. It is subjected to solar UV/EUV radiation that varies continuously, and it exchanges mass, momentum, and energy with the lower atmosphere and magnetosphere. At high-latitudes, plasma convection, particle precipitation, and Joule heating are the main sources of momentum and energy for the I-T system, and all of the global I-T models include these processes. However, if these drivers are not properly/rigorously described, then the I-T model simulations can display significant errors. Despite this problem, the physics underlying the I-T climatology has been clearly established, and the global I-T models have been able to reproduce the major I-T features. However, the I-T models have been less successful in modeling weather features, especially when attempting long-term forecasts.

In addition to the need to properly describe the drivers of the I-T system, there are other problems connected with the global I-T models that need to be addressed if more reliable specifications and forecasts are desired. Some of the problems are that the coupled global models are usually based on relatively simple mathematical formulations, the spatial and temporal resolutions are coarse, many of the parameters in the models are uncertain, the coupling between the models is incomplete, and there is missing physics in all of the global models.

If the ionosphere simulated by a global I-T model is not correct, then the resulting thermosphere will be wrong and vice versa. This problem can be illustrated with the aid of the National Center for Atmospheric Research (NCAR) thermosphere-ionosphere nested grid (TING) model and the USU GAIM-GM data assimilation model [*Jee et al.*, 2007, 2008]. The NCAR TING model was run in its "standard" coupled mode for the period 1–4 April 2004, which contained both quiet and disturbed periods. The Utah State University Global Assimilation of Ionospheric Measurements - Gauss Markov (USU GAIM-GM) data assimilation model was run

Modeling the Ionosphere-Thermosphere System
Geophysical Monograph Series 201

10.1029/2012GM001351

for the same period using slant TEC from ground receivers, bottomside N_e profiles from ionosondes, and in situ N_e densities along DMSP satellite orbits. As expected, the TING and GAIM-GM ionospheres were significantly different, particularly during disturbed times. Since the GAIM-GM model results were consistent with the available measurements, its reconstructed ionosphere is expected to be more realistic than that obtained from the coupled I-T TING ionosphere. To get a feel for what a different, and more realistic, ionosphere would do to the TING thermosphere, the TING model was rerun with the GAIM-GM ionosphere supplied to it at each TING time step in order to see the effect on the thermosphere of using a different ionosphere. There were large neutral wind, temperature, and composition differences when the GAIM-GM ionosphere was used in place of the self-consistent TING ionosphere, with T_n increases as large as 40% (409 K).

In the GAIM-TING study described above, the main problem with the "standard" TING simulation was probably related to the use of empirical plasma convection and particle convection models for the high-latitude drivers. Empirical models are not capable of describing high-latitude weather features, and the uncertainty in the high-latitude drivers can produce the largest errors in global I-T simulations, particularly during geomagnetic storms.

In addition, concerted efforts have been made to compare global, physics-based I-T models. In the Equatorial PRIMO (Problems Related to Ionospheric Models and Observations) study [*Fang et al.*, 2013], 12 models were compared for the same geophysical conditions in order to see how well the models reproduced the equatorial ionization anomaly (EIA). N_mF_2 versus latitude was compared at selected times. Typically, the spread in model results was more than a factor of 2 and was as large as a factor of 5. In general, the performance of the coupled models was worse than the stand-alone models; the coupled models had difficulty in describing the latitudinal variation of the EIA. There was also a coupling energetics and dynamics of atmospheric regions challenge for a systematic quantitative comparison of physics-based I-T models with observations; eight global models were evaluated. Nine events (two strong and four moderate storms, three quiet periods), three parameters (N_mF_2, h_mF_2, vertical drifts), and all latitudes were considered [*Shim et al.*, 2011]. As expected, no model ranked the best when all events, parameters, and latitudes were taken together. The physics-based I-T models frequently displayed significant differences from each other and from the data.

As noted above, there are many reasons why the global physics-based I-T models have problems. Here the focus will be on "some" of the physics that is missing in the global physics-based models, and therefore, this study is by no means complete. Other issues, such as instabilities, turbulence, uncertain parameters, numerical techniques, etc., will be addressed in other papers in this monograph. Ten topics relevant to missing physics have been selected as examples. Some of the topics are primarily important in local regions and, therefore, are relevant to local weather, whereas others are important for global I-T weather simulations. Subsections 2.6, 2.7, and 2.8 provide examples of the problems that arise when relatively simple mathematical formulations are used in global modeling.

2. MISSING PHYSICS IN GLOBAL PHYSICS-BASED IONOSPHERE-THERMOSPHERE MODELS

In what follows, some of the physical processes that are not included in most of the global physics-based I-T models will be highlighted. The physics may not be included in the I-T models for several reasons: there are insufficient data to warrant its inclusion, it is only applicable in a local geographical domain, the global model resolution is too coarse to incorporate the physics, it is too difficult to include it, an entirely new I-T model needs to be developed to include the physics, etc. With this in mind, it should be noted that a major advance in I-T modeling has been made during the last three decades, and the next major advance will come when the missing physics is included in the global physics-based I-T models.

2.1. Polar Wind and Auroral Ion Outflow

Figure 1 shows processes that affect the polar wind and auroral ion outflow at high latitudes. Most of these processes have been included in recent ionosphere-polar wind simulations [*Barakat and Schunk*, 2006], but the continual loss of plasma due to the polar wind and energetic ion outflow is not taken into account in the global I-T models. Typically, the upper boundary condition adapted in these global models allows the plasma to flow upward, when the electron and ion temperatures increase, and then downward, when the temperatures decrease, so that there is no net loss of plasma. However, the continual loss of plasma due to the polar wind and auroral ion outflow is significant and should have an appreciable effect on the I-T system. The H^+ outflow varies from about 1 to 5×10^8 cm^{-2} s^{-1}, and the O^+ outflow can be as large as $1–2 \times 10^9$ cm^{-2} s^{-1} in the auroral oval and during geomagnetic storms [cf. *Schunk*, 2007]. Unfortunately, the outflow is not uniform; there are propagating and stationary polar wind jets, polar wind tongues that extend across the polar cap, pulsating geomagnetic storms, flickering aurora, auroral arcs, etc. The nonuniform and continuous plasma outflow needs to be taken into account in the global I-T models if more reliable model predictions are desired.

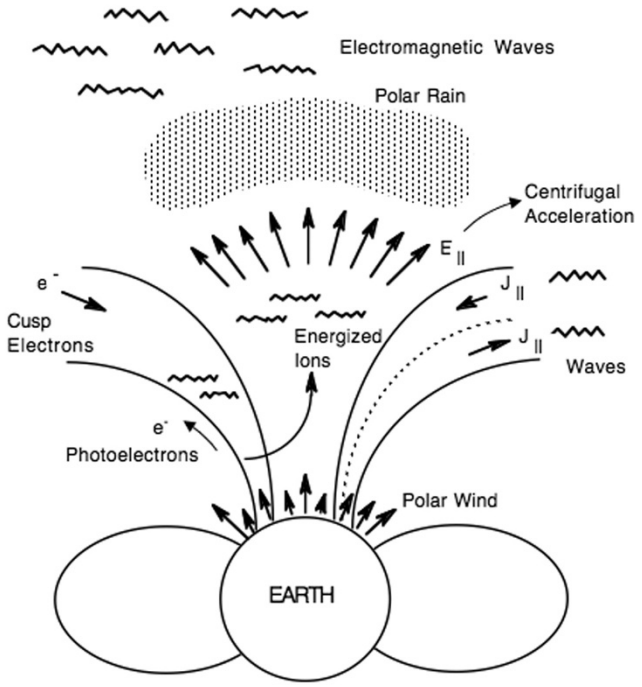

Figure 1. A schematic diagram showing the processes that affect the polar wind and energetic ion outflow from the ionosphere at high latitudes. From *Schunk and Sojka* [1997].

2.2. Downward Electron Heat Flow in the Polar Cap

As the polar wind plasma flows up and out of the topside ionosphere, it also interacts with the overlying polar rain. The energy gained by the polar wind electrons from their interaction with the hot polar rain electrons is subsequently conducted down into the underlying ionosphere, which acts to increase ionospheric electron temperatures [*Schunk et al.*, 1986]. The elevated electron temperatures then affect the ion temperatures and densities. Deductions based on model-measurement comparisons indicate that the downward electron heat flux varies from 0.5 to 1.5 $\times$ 10^{10} eV cm^{-2} s^{-1} over a range of solar cycle, seasonal, and geomagnetic activity conditions [*Bekerat et al.*, 2007]. Recently, time-dependent ionosphere model [*Schunk*, 1988; *Sojka*, 1989] simulations have been conducted of the effect that downward electron heat flows have on the high-latitude ionosphere [*David et al.*, 2011]. Three topside electron heat flux values were adopted in three separate simulations (0.0, 0.5, and 1.5 $\times$ 10^{10} eV cm^{-2} s^{-1}). Relative to the no heat flux case, the largest downward electron heat flow produced N_mF_2 changes of up to a factor of 10 in some regions of the polar cap. This effect is not included in most of current global I-T models.

2.3. Thermoelectric Heat Flow in Return Current Regions

In the ionosphere, the flow of heat is usually described by thermal conduction. In this case, $\mathbf{q} = -\lambda\nabla T$, where $\mathbf{q}$ is the heat flow vector, λ is the thermal conductivity, and T is the temperature. However, an electron heat flow can occur in response to both an electron temperature gradient (thermal conduction) and an electron current (thermoelectric heat flow). Therefore, in auroral return current regions, the electron heat flow along geomagnetic field lines is given by $\mathbf{q} = -\lambda\nabla T - \beta\mathbf{J}$, where β is the thermoelectric coefficient, and $\mathbf{J}$ is the field-aligned ionospheric return current. *Schunk et al.* [1987] studied the effect of ionospheric return currents on auroral electron temperatures for different seasonal, solar cycle, and upper boundary conditions. They found that thermoelectric heat flow is important for current densities greater than 10^{-5} A m^{-2} and that thermoelectric heat flow corresponds to an upward transport of electron energy. The upward transport of energy can result in electron temperatures that decrease with altitude, as shown in Figure 2. It is apparent that thermoelectric heat flow can be significant, but it is not included in the existing global I-T models.

2.4. Ion Temperature Anisotropy

When the convection electric field in the ionosphere is greater than about 50 mV m^{-1}, two processes occur. First, there is a rapid conversion of O^+ into NO^+, with the result that NO^+ becomes an important ion in the *F* region [*Schunk et al.*, 1975]. This rapid conversion is a consequence of the energy dependence of the $O^+ + N_2$ chemical reaction, and this process is included in all (or nearly all) of the global I-T models. However, in addition to the conversion of O^+ into NO^+, the ion temperature becomes anisotropic with the perpendicular temperature ($T_{i\perp}$) greater than the parallel temperature ($T_{i\parallel}$). Therefore, $T_{i\parallel}$ should be used in the ion momentum equation along the magnetic field, not T_i. Since T_i is greater than $T_{i\parallel}$, the use of T_i in the ion momentum equation results in an overestimation of the plasma density scale height above the *F* region peak (Figure 3). For a 100 mV m^{-1} electric field, the electron density at 600 km can be more than a factor of 2 too large if T_i is used in the momentum equation instead of $T_{i\parallel}$. This ion temperature anisotropy is probably not taken into account in most of the global I-T models.

2.5. Subauroral Red (SAR) Arcs

SAR arcs correspond to 6300 A emission that is confined to a narrow latitudinal region just equatorward of the auroral oval [cf. *Schunk and Nagy*, 2009]. The emission occurs during elevated magnetic activity and can be seen in both

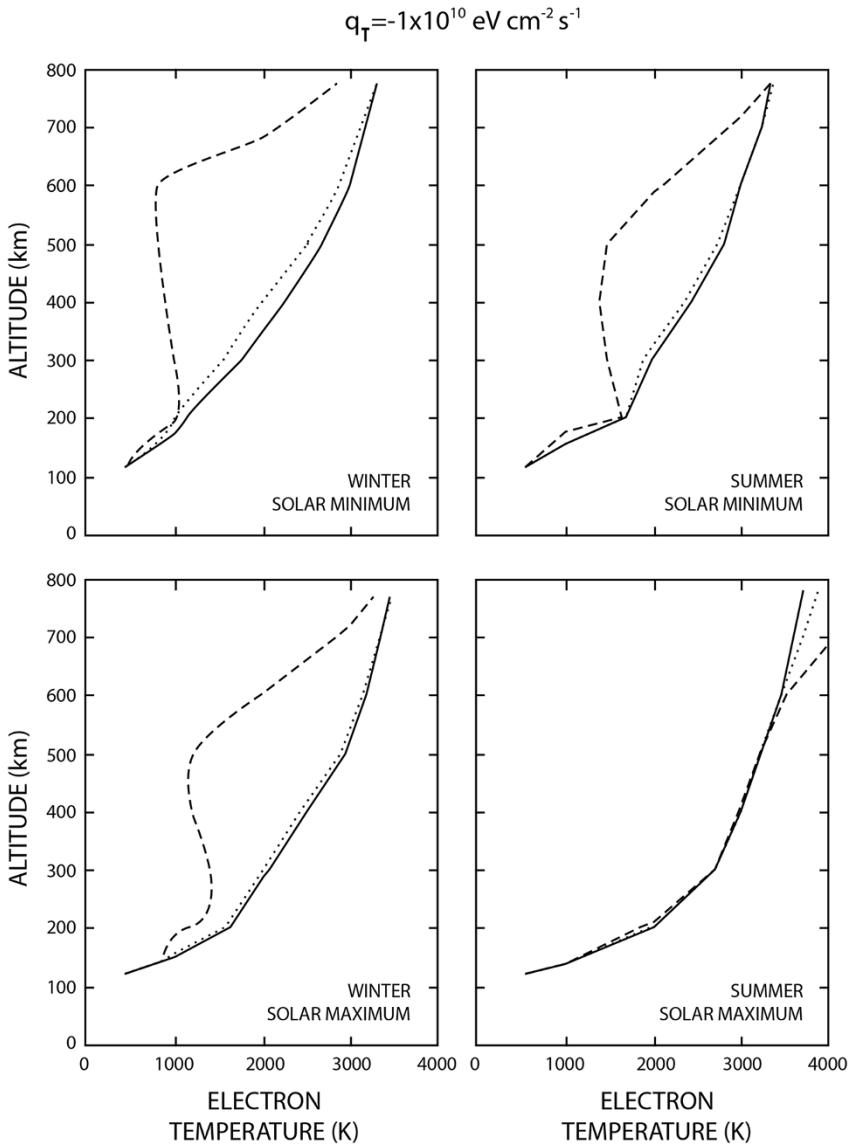

Figure 2. Electron temperature profiles for three values of the field-aligned auroral return current for winter and summer conditions at both solar minimum and maximum. The field-aligned current values are 0 (solid curves), -1×10^{-5} (dotted curves), and -5×10^{-5} (dashed curves) A m^{-2}. An upper boundary (800 km) heat flux of -1×10^{10} eV cm^{-2} s^{-1} was used for these simulations to account for the interaction of the ionospheric electrons with the hot polar rain electrons. From *Schunk et al.* [1987].

hemispheres and at all longitudes. The peak emission rate typically is localized in the 350–400 km altitude range. The emission originates from the interaction of the ring current with plasma on outer plasmaspheric flux tubes. Through Coulomb collisions and wave-particle interactions, energy is transferred from the ring current to the thermal electrons, and then, the energy is conducted down into the ionosphere. The elevated electron temperature is then capable of exciting the oxygen red line.

SAR arcs are useful for illustrating an important process that is not included in all of the global coupled I-T models. This process involves N_2 vibrational excitation. In addition to exciting the oxygen red line, elevated electron temperatures can increase the population of vibrationally excited N_2, which then acts to increase the rate of the $O^+ + N_2 \Rightarrow NO^+ + N$ reaction. The net result can be a rapid conversion of O^+ into NO^+. Figure 4 shows the possible effect of vibrationally excited N_2 on the N_e profile via the associated O^+ to NO^+ conversion

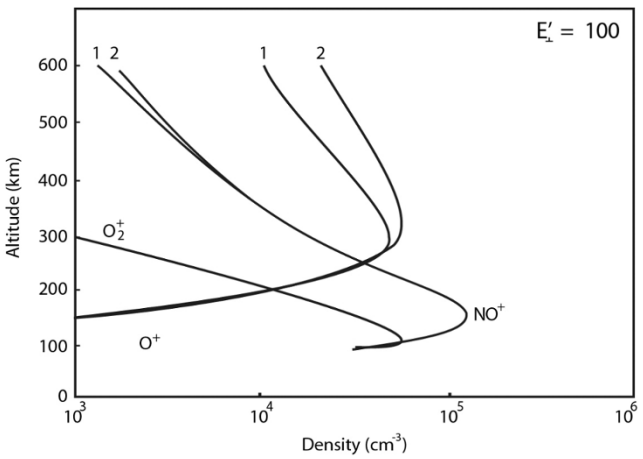

Figure 3. Ion density profiles calculated for a daytime high-latitude ionosphere subjected to a 100 mV m^{-1} electric field. The curves labeled 2 were calculated with T_i, and the curves labeled 1 were calculated with $T_{i\|}$. From *Schunk et al.* [1975].

process. The top panel shows the adopted SAR arc T_e profile, and the bottom panel shows the calculated N_e. Note that N_2 vibrational excitation can have a dramatic effect on the shape of the N_e profile. Since excited N_2 molecules are prevalent in and around the auroral oval, these molecules need to be taken into account in the global coupled I-T models.

2.6. Collisionless Plasma Flow

The current global ionosphere and ionosphere-plasmasphere models [*Bailey and Sellek*, 1990; *Millward et al.*, 1996; *Richards and Torr*, 1996; *Schunk et al.*, 2004] are based on relatively simple mathematical formulations. Specifically, the adopted continuity, momentum, and energy equations are simplified by ignoring nonlinear and/or complicated terms. It is also assumed that the plasma is collision dominated, which means that the momentum equation reduces to a diffusion equation (see section 2.7 for further details).

With regard to the energy equation, either an empirical model is adopted for the plasma temperatures or collision-dominated energy and heat flow equations are solved. With the collision-dominated transport formulation, the temperatures are isotropic, and the heat flow is simply given by the collision-dominated expression $\mathbf{q} = -\lambda \nabla T$. However, above about 3000 km, the plasma becomes collisionless in the polar wind, along SAR arc and plasmapause field lines, and in the plasmasphere after geomagnetic storms [*Demars and Schunk*, 1987a, 1987b]. When the plasma becomes collisionless, the use of isotropic temperatures and collision-dominated thermal conductivities is not valid. In a collisionless plasma, there are different species temperatures parallel and perpendicular to the magnetic field, and there are separate heat flow vectors for the transport of parallel and perpendicular energies. Hence, a *rigorous formulation* of the plasma flow requires a kinetic, semikinetic, generalized transport, or macroscopic particle-in-cell approach, all of which are difficult to implement for a global coupled I-T-P model. An example of collisionless heat flow is shown in Figure 5, where the heat flow vectors (parallel to **B**) for parallel and perpendicular energies are plotted versus altitude for SAR arc conditions [*Demars and Schunk*, 1986]. The simulation was from the

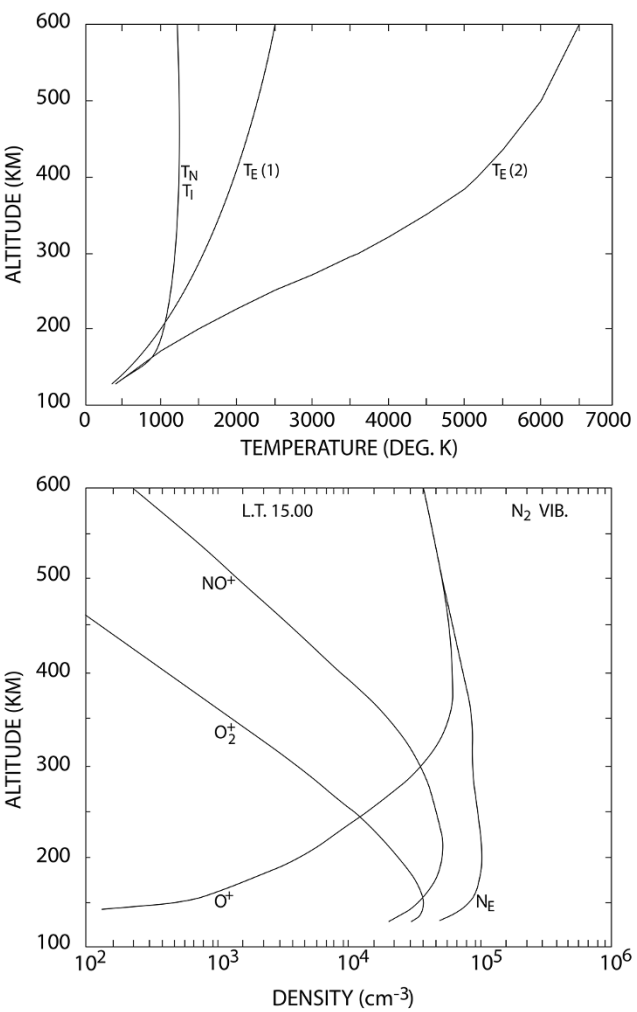

Figure 4. (top) Altitude profiles of the adopted electron, ion, and neutral temperatures used in subauroral red (SAR) arc calculations; $T_e(1)$ and $T_e(2)$ are the electron temperatures outside and inside the SAR arc, respectively. (bottom) Calculated ion and electron density profiles in a SAR arc including the effect of N_2 vibrational excitation and the associated increase in the $O^+ + N_2 \Rightarrow NO^+ + N$ reaction. From *Raitt et al.* [1976].

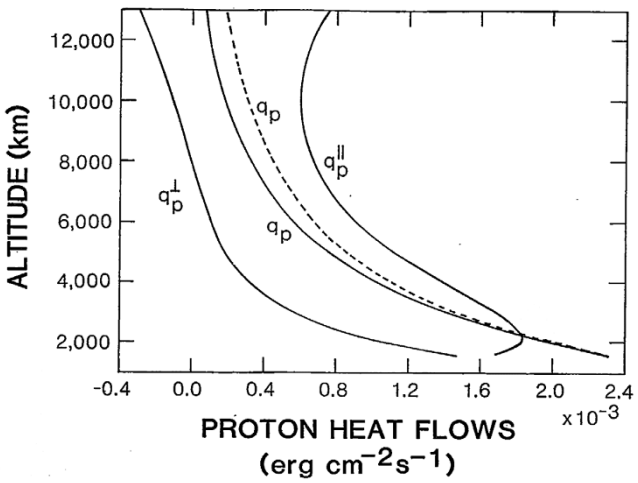

Figure 5. Proton heat flows along **B** for the transport of parallel energy ($q_p^{\parallel}$), perpendicular energy ($q_p^{\perp}$), and total energy (q_p) along a SAR arc field line, where $q_p = (q_p^{\parallel} + 2q_p^{\perp})/2$. Solid curves correspond to the solution of the 16-moment bi-Maxwellian transport equations. The dashed curve is not relevant to the discussion in the paper. From *Demars and Schunk* [1986].

solution of the 16-moment bi-Maxwellian transport equations. Note that with the more rigorous mathematical formulation, the density, drift velocity, and temperature solutions are significantly different from those obtained from the simplified diffusion and heat conduction equations commonly used in global coupled I-T-P models [see *Demars and Schunk*, 1986, 1987a, 1987b].

2.7. Ionosphere-Plasmasphere Coupling

As noted above, the four well-known physics-based global models of the coupled ionosphere-plasmasphere are based on a relatively simple diffusion formulation, which means that the nonlinear inertial term in the momentum equation ($\partial\mathbf{u}/\partial t + \mathbf{u}\cdot\nabla\mathbf{u}$) is not included [*Bailey and Sellek*, 1990; *Richards and Torr*, 1996; *Millward et al.*, 1996; *Schunk et al.*, 2004; *Scherliess et al.*, 2004]. The neglect of this term is useful for numerical reasons, but there are two negative consequences. Specifically, wave phenomena are not included, and the model cannot rigorously describe supersonic flow. The latter restriction is serious because after a geomagnetic storm, the upflow from the ionosphere that refills the depleted plasmasphere is supersonic. The neglect of the nonlinear inertial term, which acts to slow the upflow, not only means that the altitude profiles are wrong but that the refilling rate is too fast.

Another simplification is that none of the global I-P models couple to the ring current via wave-particle interactions, which means that the models do not properly describe the electron and ion thermal structure in the plasmasphere. Typically, the temperatures in the outer plasmasphere obtained from the global I-P models are too low (~4000–5000 K), whereas measurements indicate they are typically 8000–10,000 K [*Titheridge*, 1998]. To circumvent this problem, *Schunk et al.* [2004] adopted the empirical plasmasphere temperature model developed by *Titheridge* [1998]. Although this temperature model is based on an extensive satellite database, it is simplified in that it is a static empirical model.

Typically, the transport equations adopted to describe plasmasphere refilling determine the physics that is obtained. As noted above, a global I-P model that is based on a momentum equation that includes the nonlinear inertial term produces a different solution than that obtained from the four global I-P models that ignore this term (diffusion approximation), especially after geomagnetic storms. However, more advanced mathematical formulations can still lead to other completely different solutions [*Rasmussen and Schunk*, 1988]. In this latter study, the plasmasphere refilling was simulated with both a single-stream and a two-stream H^+ model. Specifically, the authors solved the H^+ continuity and momentum equations along a closed geomagnetic flux tube for a depleted plasmasphere. The momentum equation included the nonlinear inertial term so that wave phenomena and supersonic plasma flows could be properly modeled. In one simulation, a single H^+ stream was assumed, and in the second simulation, two independent H^+ streams were assumed (one from the Northern Hemisphere and one from the Southern Hemisphere). Figure 6 compares the plasmasphere refilling for the two cases. In both cases, the upflow is supersonic. For the single-stream simulation, there is only one H^+ velocity at each location along the flux tube, and when the counterstreaming H^+ flows from the conjugate hemispheres meet, a zero velocity results, and a pair of shocks is automatically triggered. The shocks then propagate toward lower altitudes, creating high-density plasma between the shock pair. In this case, the plasmasphere fills from the top down. On the other hand, for the case when the refilling is modeled with separate northern and southern H^+ streams, the counterstreaming supersonic flows penetrate each other, and shocks do not form. In this case, the plasmasphere fills from the bottom up. Hence, totally different results are obtained depending on how the plasmasphere refilling is modeled, with more rigorous mathematical formulations yielding more reliable solutions.

2.8. Plasma and Neutral Density Structures

Troposphere weather features can take on global characteristics, but most of the weather features are more localized, including hurricanes, tornados, snowstorms, fog banks,

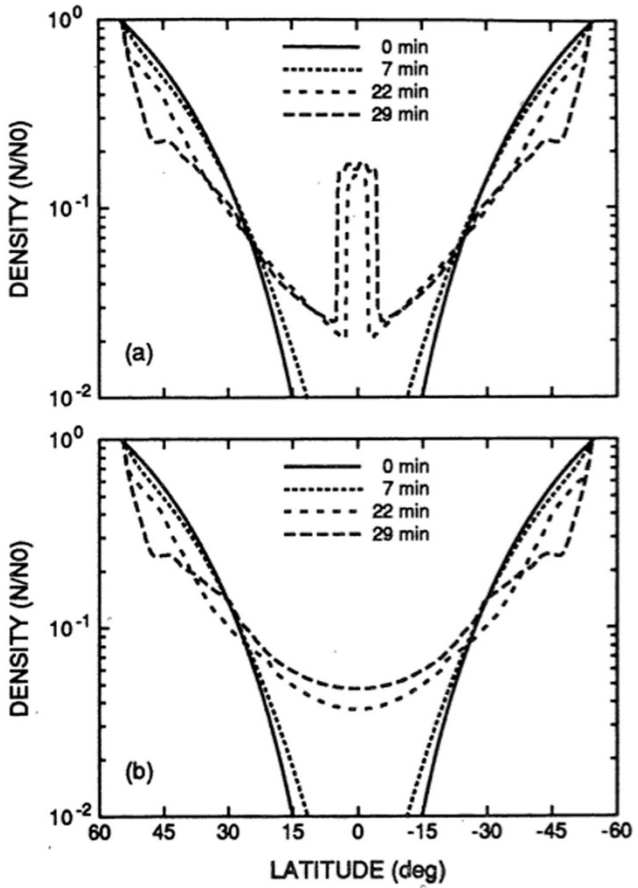

Figure 6. Electron density as a function of dipole latitude for the (a) single-stream H^+ model and for the (b) two-stream H^+ model. The multiple curves show the temporal evolution of the electron density as the flux tube fills, with the 0 min curves corresponding to the start of the simulations. From *Rasmussen and Schunk* [1988].

torrential rains, and sleet/hail. It is these more localized weather features that have the greater impact on human activities. Likewise, in addition to global characteristics, the weather features in the I-T-E system also displays more localized features, including mesoscale (50–1000 km) density structures. At high latitudes, the mesoscale plasma structures include tongues of ionization, aurora and boundary blobs, theta aurora, subauroral ion drift events, propagating plasma patches, and sun-aligned polar cap arcs. At middle and low latitudes, the structures include storm-enhanced density ridges and equatorial plasma bubbles. Examples of neutral density/wind structures include the cusp neutral fountain, propagating atmospheric holes, and supersonic neutral wind gusts. These localized features can have a significant impact on global-scale flows, and the resolution in the global I-T models needs to be fine enough to automatically include mesoscale I-T structures.

An important point to note about I-T structures is that if one observes a plasma structure, there is an associated neutral structure, and vice versa. For example, Figures 7a and 7b show I-T simulation results for the effect on the thermosphere of a series of propagating plasma patches [*Ma and Schunk*, 2001]. In this simulation, the width (200 km), length (1000 km), spacing (200 km), direction of propagation (antisunward), and density factor (10 above the background) of the cigar-shaped plasma patches were determined from measurements [*Fukui et al.*, 1994]. In the simulation, a diurnally reproducible, global I-T was first calculated, and then, at 02:65 UT (t = 0), the series of propagating plasma patches was introduced in the southern polar region. The patches were imposed, one at a time, near the cusp at a half-hour interval, and then, they propagated across the polar cap at the prevailing convection speed, yielding a 200 km separation between the plasma patches. The simulation results are for moderate solar activity (F10.7 = 150), a two-cell convection pattern with a 100 kV cross-tail magnetospheric potential, a Gaussian-shaped N_e profile in the horizontal direction, and a peak-to-background N_e ratio of 10.

In Figure 7a, the snapshot is for t = 3 h, which is 3 h after the first plasma patch was introduced. Figure 7a shows the N_e distribution at 300 km, the neutral density perturbation ($\Delta\rho$) at 300 km, and $\Delta\rho$ via a 2-D (altitude and latitude) day-night cut across the polar cap through the center of the series of plasma patches. In general, propagating plasma patches act as a snowplow, creating a hole in the thermosphere in and behind the individual plasma patches and neutral density enhancements in front of the patches. For plasma patches that have a factor of 10 density enhancement above the background plasma density, there is a 30%–35% neutral density perturbation due to the propagating plasma patches. The neutral disturbance moves along with the propagating plasma patches and is characterized by an increased wind speed (Δu > 100 m s^{-1}), a temperature enhancement ($\Delta T \approx$ 100–300 K), neutral gas upwelling, and O/N_2 composition changes. The propagating plasma patches also excite waves in the thermosphere that propagate away from the neutral disturbance, as shown in Figure 7a, which is for t = 3 h, and in Figure 7b, which is for t = 4.41 h.

2.9. Neutral Rain on the Thermosphere

As the polar wind and auroral H^+ and O^+ ions flow upward, they can undergo charge exchange reactions with the background thermal and energetic neutrals, thereby creating upflowing H_s and O_s stream neutrals [*Gardner and Schunk*, 2004, 2005]. The streaming neutrals are superthermal because at creation, they have the same velocity and energy as their parent ions. Upflowing H_s and O_s stream neutrals are

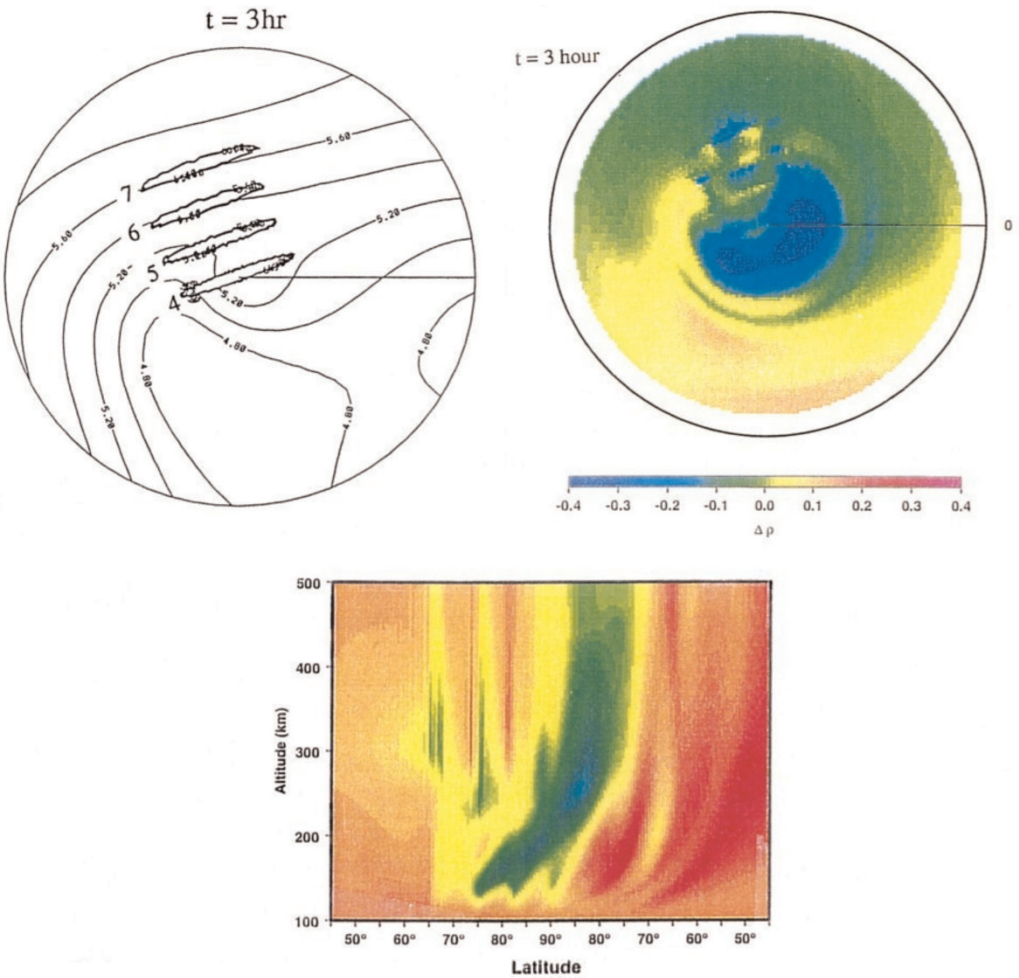

Figure 7a. Effect of multiple propagating plasma patches on the thermosphere at t = 3 h. (left top) The N_e distribution at 300 km in units of $\log_{10}N_e$ (cm^{-3}), (right top) the neutral density perturbation at 300 km, and (bottom) the neutral density perturbation versus altitude and latitude across the polar cap. From *Ma and Schunk* [2001].

also created on closed magnetic flux tubes, particularly after the tubes are depleted by geomagnetic storms. At all latitudes, the H_s stream neutrals have sufficient energy to escape, but most of the O_s stream neutrals do not have enough energy to escape and then rain down on the I-T system. The neutral rain provides a global energy source for the thermosphere as the downstreaming neutrals collide with the background thermal neutrals. This effect is not included in the current global I-T models, but the exact effect of this process has not been fully elucidated.

2.10. Lower Atmosphere Wave Effects

At low altitudes, the I-T system is continually subjected to planetary, tidal, and gravity waves that propagate upward from the lower atmosphere. These waves then affect the neutral winds and electrodynamics in the *E* region. They also interact with the waves generated internally in the thermosphere. The upward propagating planetary, tidal, and large-scale gravity waves can be described by models that extend from the Earth's surface to the upper thermosphere. However, high-resolution I-T models are needed to properly account for small-scale gravity waves and for the consequent wave-wave coupling in the thermosphere. This work has only recently begun (see other papers in this monograph).

3. SUMMARY

Community-wide initiatives have shown that the output of global physics-based I-T models can be significantly different

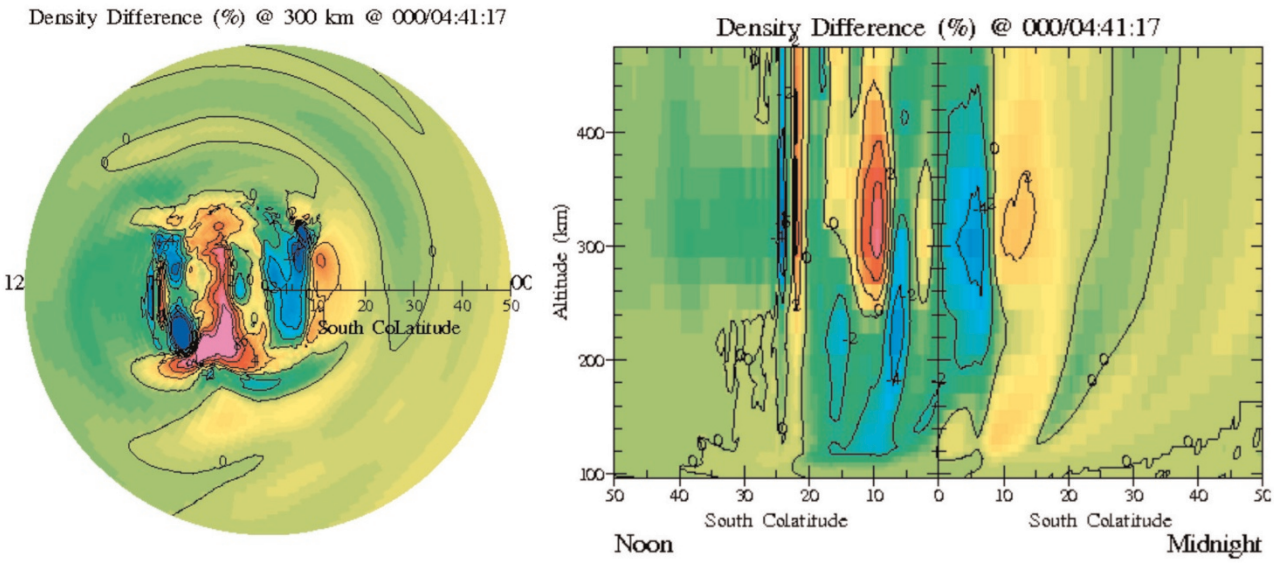

Figure 7b. Snapshot at t = 4.41 h of the neutral density perturbation due to multiple propagating plasma patches. The neutral perturbation is shown (left) at 300 km and (right) as a function of altitude and latitude across the polar cap. From *Schunk et al.* [2008].

from each other and from the measurements when they are compared for the same geophysical case. As noted above, there are numerous problems with the existing I-T models, but in this paper, the focus was on some of the physics that is missing from the global I-T models. At high latitudes, the models should be expanded to include polar wind and auroral ion outflow, the downward electron heat at the upper boundary in the polar cap, thermoelectric heat flow in the return current regions, and the ion temperature anisotropy due to strong electric fields. Near the plasmapause and in SAR arcs, the electron density effects associated with N_2 vibrational excitation need to be taken into account. In I-T models that couple to the plasmasphere, the plasma becomes collisionless above about 3000 km, and the heat flow is not governed by the standard thermal conductivity. In addition, during plasmasphere refilling after geomagnetic storms, a multistream formulation is needed for each ion species. In general, the resolution in the global I-T models needs to be improved so that mesoscale plasma and neutral density structures can be taken into account in a self-consistent way. The improved resolution is also needed to take account of the upward propagating gravity waves from the lower atmosphere. Another process that should be included is the neutral rain on the thermosphere.

Ten topics relevant to missing physics in I-T models were selected as examples. However, some of the topics are primarily important in local regions and, therefore, are relevant to local weather, whereas others are important for global I-T weather simulations. The missing physics relevant to local weather simulations includes thermoelectric heat flow in return current regions (section 2.3), ion temperature anisotropies in regions with large electric fields (section 2.4), SAR arcs (section 2.5), and plasma and neutral density structures (section 2.8). The missing physics that should have a significant effect on global I-T weather simulations includes polar and auroral ion outflow (section 2.1), downward electron heat flow in the polar cap (section 2.2), ionosphere-plasmasphere coupling (section 2.7), neutral rain on the thermosphere (section 2.9), and lower atmosphere wave effects (section 2.10). However, the cumulative effect of plasma and neutral density structures (section 2.8) may also affect the global mean circulation and temperature of the thermosphere [*Smith*, 2000].

In general, the global I-T and I-T-P models that are based on diffusion and hydrodynamic (fluid) formulations are not valid when the plasma and neutral gas become collisionless, which occurs above about 3000 km for the ionosphere-polar wind and ionosphere-plasmasphere models, and above about 500 km for the thermosphere models. As a consequence, the densities, drift velocities, temperatures, and heat flows, as well as their variations with altitude, are wrong if a diffusion or hydrodynamic formulation is used in the collisionless region.

The focus of this work was on "some" of the physics that is missing in the global physics-based models, and therefore, the examples of missing physics that were presented here do not constitute a complete list. Other issues, such as instabilities, turbulence, uncertain parameters, numerical techniques, etc., are addressed in other papers in this monograph.

REFERENCES

Bailey, G. J., and R. Sellek (1990), A mathematical model of the Earth's plasmasphere and its application in a study of He+ at *L*=3.0, *Ann. Geophys.*, *8*, 171–190.

Barakat, A. R., and R. W. Schunk (2006), A three-dimensional model of the generalized polar wind, *J. Geophys. Res.*, *111*, A12314, doi:10.1029/2006JA011662.

Bekerat, H., R. W. Schunk, and L. Scherliess (2007), Estimation of the high-latitude topside electron heat flux using DMSP plasma density measurements, *J. Atmos. Sol. Terr. Phys.*, *69*, 1029–1048.

David, M., R. W. Schunk, and J. J. Sojka (2011), The effect of downward electron heat flow and electron cooling processes in the high-latitude ionosphere, *J. Atmos. Sol. Terr. Phys.*, *73*(16), 2399–2409, doi:10.1016/j.jastp.2011.08.009.

Demars, H. G., and R. W. Schunk (1986), Solutions to bi-Maxwellian transport equations for SAR-arc conditions, *Planet. Space Sci.*, *34*, 1335–1348.

Demars, H. G., and R. W. Schunk (1987a), Temperature anisotropies in the terrestrial ionosphere and plasmasphere, *Rev. Geophys.*, *25*, 1659–1679.

Demars, H. G., and R. W. Schunk (1987b), Comparison of solutions to bi-Maxwellian and Maxwellian transport equations for subsonic flow, *J. Geophys. Res.*, *92*, 5969–5990.

Fang, T.-W., et al. (2013), Equatorial-PRIMO (Problems Related to Ionospheric Models and Observations), in *Modeling the Ionosphere/Thermosphere System*, *Geophys. Monogr. Ser.*, doi:10.1029/2012GM001280, this volume.

Fukui, K., J. Buchau, and C. Valladares (1994), Convection of polar cap patches observed at Qaanaaq, Greenland during the winter of 1989–1990, *Radio Sci.*, *29*(1), 231–248.

Gardner, L. C., and R. W. Schunk (2004), The neutral polar wind, *J. Geophys. Res.*, *109*, A05301, doi:10.1029/2003JA010291.

Gardner, L. C., and R. W. Schunk (2005), Global neutral polar wind model, *J. Geophys. Res.*, *110*, A10302, doi:10.1029/2005JA011029.

Jee, G., A. G. Burns, W. Wang, S. C. Solomon, R. W. Schunk, L. Scherliess, D. C. Thompson, J. J. Sojka, and L. Zhu (2007), Duration of an ionospheric data assimilation initialization of a coupled thermosphere-ionosphere model, *Space Weather*, *5*, S01004, doi:10.1029/2006SW000250.

Jee, G., A. G. Burns, W. Wang, S. C. Solomon, R. W. Schunk, L. Scherliess, D. C. Thompson, J. J. Sojka, and L. Zhu (2008), Driving the TING model with GAIM electron densities: Ionospheric effects on the thermosphere, *J. Geophys. Res.*, *113*, A03305, doi:10.1029/2007JA012580.

Ma, T.-Z., and R. W. Schunk (2001), The effects of multiple propagating plasma patches on the polar thermosphere, *J. Atmos. Sol. Terr. Phys.*, *63*, 355–366.

Millward, G. W., R. J. Moffett, S. Quegan, and T. J. Fuller-Rowell (1996), A coupled thermosphere-ionosphere-plasmasphere model (CTIP), in *STEP Handbook of Ionospheric Models*, edited by R. W. Schunk, pp. 239–280, Utah State Univ., Logan.

Raitt, W. J., R. W. Schunk, and P. M. Banks (1976), Ionospheric composition in SAR-arcs, *Planet. Space Sci.*, *24*, 105–114.

Rasmussen, C. E., and R. W. Schunk (1988), Multi-stream hydrodynamic modeling of interhemispheric plasma flow, *J. Geophys. Res.*, *93*, 14,557–14,565.

Richards, P. G., and D. G. Torr (1996), The field line interhemispheric plasma model, in *STEP Handbook of Ionospheric Models*, edited by R. W. Schunk, pp. 239–280, Utah State Univ., Logan.

Scherliess, L., R. W. Schunk, J. J. Sojka, and D. C. Thompson (2004), Development of a physics-based reduced state Kalman filter for the ionosphere, *Radio Sci.*, *39*, RS1S04, doi:10.1029/2002RS002797.

Schunk, R. W. (1988), A mathematical model of the middle and high latitude ionosphere, *Pure Appl. Geophys.*, *127*, 255–303.

Schunk, R. W. (2007), Time-dependent simulations of the global polar wind, *J. Atmos. Sol. Terr. Phys.*, *69*, 2028–2047.

Schunk, R. W., and A. F. Nagy (2009), *Ionospheres*, 2nd ed., Cambridge Univ. Press, Cambridge, U. K.

Schunk, R. W., and J. J. Sojka (1997), Global ionosphere-polar wind system during changing magnetic activity, *J. Geophys. Res.*, *102*, 11,625–11,651.

Schunk, R. W., P. M. Banks, and W. J. Raitt (1975), Effect of electric fields on the daytime high-latitude E- and F-regions, *J. Geophys. Res.*, *80*, 3121–3130.

Schunk, R. W., J. J. Sojka, and M. D. Bowline (1986), Theoretical study of the electron temperature in the high latitude ionosphere for solar maximum and winter condition, *J. Geophys. Res.*, *91*, 12,041–12,054.

Schunk, R. W., J. J. Sojka, and M. D. Bowline (1987), Theoretical study of the effect of ionospheric return currents on the electron temperature, *J. Geophys. Res.*, *92*, 6013–6022.

Schunk, R. W., et al. (2004), Global Assimilation of Ionospheric Measurements (GAIM), *Radio Sci.*, *39*, RS1S02, doi:10.1029/2002RS002794.

Schunk, R. W., L. Gardner, L. Scherliess, D. C. Thompson, and J. J. Sojka (2008), Effect of lower atmospheric waves on the ionosphere and thermosphere, paper presented at the 2008 Ionospheric Effects Symposium, JMG Assoc., Natl. Tech. Inf. Serv., Springfield, Va.

Shim, J. S., et al. (2011), CEDAR electrodynamics thermosphere ionosphere (ETI) challenge for systematic assessment of ionosphere/thermosphere models: NmF2, hmF2, and vertical drift using ground-based observations, *Space Weather*, *9*, S12003, doi:10.1029/2011SW000727.

Smith, R. W. (2000), The global-scale effect of small-scale thermospheric disturbances, *J. Atmos. Sol. Terr. Phys.*, *62*, 1623–1628.

Sojka, J. J. (1989), Global scale, physical models of the F region ionosphere, *Rev. Geophys.*, *27*, 371–403.

Titheridge, J. E. (1998), Temperatures in the upper ionosphere and plasmasphere, *J. Geophys. Res.*, *103*, 2261–2277.

R. W. Schunk, Center for Atmospheric and Space Sciences, Utah State University, Logan, UT 84322-4405, USA. (robert.schunk@usu.edu)

Physical Characteristics and Modeling of Earth's Thermosphere

Tim Fuller-Rowell

CIRES University of Colorado, Boulder, Colorado, USA

NOAA Space Weather Prediction Center, Boulder, Colorado, USA

Earth's neutral thermosphere extends from roughly 100 to 600 km altitude and comprises more than 99% of the medium. The lower limit of the thermosphere is the mesopause, where the average temperature profile starts to increase sharply, heated by absorption of solar ultraviolet (UV) radiation. The thermosphere is collision dominated enabling the gas laws and fluid equations to be used. The upper limit of the thermosphere, the exobase, is the level were fluid properties break down. Hydrostatic balance and pressure coordinates are often invoked. In addition to advection, pressure gradients, Coriolis, and diffusion, the presence of plasma and the magnetic field give rise to ion drag and Joule heating. In the lower 10 or 20 km, turbulence mixes momentum, potential temperature, and the main O_2 and N_2 species. At higher altitudes, molecular diffusion allows species to separate out depending on their molecular mass, with lighter species above and heavier species below. Solar radiation also dissociates molecular oxygen; the lighter atomic oxygen becomes the third major species, which dominates in the upper thermosphere. Hydrostatic balance can support large vertical winds and the propagation of large-scale gravity waves. Thermal expansion does not change the relative contribution of species on pressure levels, but the global circulation transports species vertically and horizontally, enhancing heavier species in regions of upwelling and lighter species in regions of downwelling. At high latitudes, ion drag drives high-velocity, nonlinear neutral wind vortices and can stimulate inertial resonances. Thermospheric winds, temperature, and composition have a strong impact on the ionosphere.

1. INTRODUCTION

Earth's upper atmosphere is a gravitationally bound weakly ionized fluid extending from roughly 100 to 600 km altitude. More than 99% of the gas is "neutral," or not ionized, so understanding and modeling the neutral component, the thermosphere, is crucial for an adequate representation and understanding of the ionized component. The ions make up less than 1% of the total mass. This chapter describes the basic physical processes in the thermosphere, or Earth's neutral upper atmosphere, which need to be captured in a physics-based model. The thermosphere is the medium from which the ionosphere is created, and the neutral dynamics and composition is an important driver of the ionized component. The ionosphere, in turn, has important impacts on the neutral medium through ion drag and Joule heating.

The fluid properties of the neutral gas result from the frequent collisions between the atoms and molecules. Rather than having to accommodate the random nature of the forces exerted on individual gas particles, the principles of kinetic theory can be invoked so that the medium can be described

Modeling the Ionosphere-Thermosphere System
Geophysical Monograph Series 201

10.1029/2012GM001329

by the bulk properties of the fluid, such as pressure, density, temperature, and velocity. The fluid properties also enable the use of the Navier-Stokes momentum equations. The upper extent of the atmosphere is usually defined as the altitude at which the fluid approximation is no longer valid, referred to as the exobase. Below the exobase, the distance traveled or time taken between collisions is short compared to the scale sizes of interest in the dynamics and energetics of the fluid. For the Earth, this altitude is usually around 600 km, but can be higher since it depends on the gas kinetic temperature, and hence the degree of thermal expansion of the medium. It is more appropriate to state the vertical extent of the atmosphere in terms of pressure level. Most physical models of Earth's upper atmosphere are limited to a top pressure level of about 10^{-7} Pa for this reason. At lower pressures, or greater heights, the mean free path or the distance between collisions exceeds tens of kilometers, and the medium acts as free particles rather than a fluid.

2. THE GAS LAW AND HYDROSTATIC BALANCE

The frequent collisions of a gas close to thermal equilibrium enable the Maxwellian energy distribution of the individual particles to be replaced by the basic fluid properties of pressure, p, temperature, T, number density, n, and mass density, ρ, that are related by the perfect gas law:

$$p = nkT \tag{1}$$

or

$$p = \rho R \frac{T}{M} \tag{2}$$

where k and R are the Boltzmann and gas constants, respectively, and M is the molecular mass in atomic units.

The gas under the influence of the planet's gravitational force gives rise to the concept of hydrostatic balance, which states that the change in pressure with height, ∂p, is closely balanced by the weight of the fluid, $nmg\partial h$, under the action of the planet's gravitational field. The concept is expressed mathematically as

$$\partial p = -nmg\partial h \tag{3}$$

or

$$\frac{\partial p}{\partial h} = -\rho g \tag{4}$$

where m is the mean molecular mass in kilograms, h is the height, and g is the planet's gravitational acceleration. These basic equations describe the exponential decrease in gas density with altitude and introduce the concept of scale height, $H = RT/Mg$, which represents the altitude through which the gas density will decrease by a factor of $1/e$. Most of the physical processes controlling the global thermosphere dynamics, energy budget, and composition can be described assuming the atmosphere is in "quasi-hydrostatic balance," which assumes vertical acceleration is small compared with gravity.

The assumption of hydrostatic balance implies that a vertical column of gas responds to a heat source instantaneously. In the real atmosphere, the information about heating at a given altitude or pressure level is transferred to other regions by acoustic gravity waves, which have speeds of hundreds of meters per second, corresponding to a time scale for adjustment of typically 5 to 10 min. This time scale is similar to the buoyancy or Brunt-Väisälä period. Treatment or understanding of dynamical time scales shorter than this period, or spatial scales less than ~50 km, has to explicitly include acoustic waves. So the physics and model described here is limited to the larger temporal and spatial scales. This chapter makes the implicit assumption of hydrostatic equilibrium and, consequently, will not cover acoustic waves and their potential impact on the thermosphere. The impact of non-hydrostatic processes during impulsive energy injection on short time scales will be addressed by *Deng and Ridley* [this volume]. During these times, vertical acceleration can be a significant fraction (20%) of the gravitational acceleration.

The assumption of quasi-hydrostatic balance enables pressure to be used as the vertical coordinate in neutral atmosphere models and enables the concept of a reduced height z^*, where $p = p_0 e^{-z^*}$, such that

$$\frac{\partial h}{\partial z^*} = H \tag{5}$$

and the height of the pressure surfaces can be evaluated by integrating from the lower boundary, h_0,

$$h = h_0 + \int H \partial z^* \tag{6}$$

and

$$\partial z^* = -\frac{\partial h}{H} = \frac{\partial p}{p} = \frac{\partial n}{n} + \frac{\partial H}{H}. \tag{7}$$

In these types of models, the horizontal pressure gradient is replaced by the horizontal gradient in the height of the pressure levels. The pressure coordinate system has several benefits. It reduces the dimensionality of the problem; simplifies the continuity equation (see below); simplifies solar and auroral absorption, since pressure surfaces are levels of constant optical depth; changes of temperature in a column of gas do not change the relative contribution of neutral

species on pressure levels; and vertical winds can be separated into physically meaningful processes (see below).

The equilibrium condition implied by hydrostatic balance, however, does not exclude the possibility of vertical winds. The assumption simply demands that the rate of heating is such that the atmosphere adjusts at a comparable rate. The term "quasi-hydrostatic balance" is the more correct expression in the case of accommodating vertical winds in the system. One component of the vertical wind is then defined as the rate of change in the height of a pressure surface in the column of gas $(\partial h/\partial t)_p$ and is termed the "barometric wind." Vertical winds in Earth's upper atmosphere of the order of 100 m s^{-1} can be accommodated within the quasi-hydrostatic assumption. The assumption of hydrostatic balance has enabled the wide use of pressure as the vertical coordinate in atmospheric models. In fact, only recently have Earth upper-atmosphere models begun to relax this assumption and explicitly include a realistic adjustment process by acoustic waves [e.g., *Ridley et al.*, 2006; *Deng et al.*, 2008; *Deng and Ridley*, this volume]. Such models are able to examine the physical response at small-scale sizes and on short time scales, albeit at the expense of increased computation.

3. CONTINUITY EQUATION

The continuity equation is also one of the most widely used and universal fluid concepts. In the pressure coordinate system, the continuity equation can be expressed as

$$\frac{\partial \omega}{\partial p} = -\nabla_p \cdot \mathbf{V} \tag{8}$$

where ω is the vertical wind in the pressure coordinate system, dp/dt, and the right-hand side represents the horizontal divergence of neutral wind, **V**, on a pressure surface p. The fluid, therefore, appears incompressible in this natural coordinate system, where horizontal divergence or convergence must be balanced by a vertical flow. This, in fact, describes the second component of vertical winds, the so-called "divergence wind." A local heat source will cause the local column of gas to thermally expand (the barometric wind), while the horizontal pressure gradients so induced will drive a divergent wind that must be balanced by a vertical flow across the pressure surfaces. The total vertical wind, V_z, in this system can be expressed as the sum of the barometric and divergence wind, $-\omega/\rho g$, components thus

$$V_z = \left(\frac{\partial h}{\partial t}\right)_p - \frac{\omega}{\rho g}. \tag{9}$$

The vertical wind becomes a diagnostic, rather than prognostic equation, and represents the reduced dimensionality of the problem.

4. LAGRANGIAN VERSUS EULERIAN FRAMES OF REFERENCE

Atmospheric models typically solve the equations in an Eulerian coordinate system fixed with respect to the Earth, usually spherical polar coordinates in radius, r, latitude, θ, and longitude, ϕ. The rate of change of a state parameter at a fixed point in the spherical polar coordinate space (r,θ,ϕ) is represented by the partial derivative $\partial/\partial t$. The partial and total derivatives are connected by the advection terms:

$$\frac{\mathrm{d}}{\mathrm{d}t} = \frac{\partial}{\partial t} + \frac{V_\theta}{r}\frac{\partial}{\partial \theta} + \frac{V_\phi}{r\sin\theta}\frac{\partial}{\partial \phi} + \omega\frac{\partial}{\partial p}. \tag{10}$$

Physically, the advection terms represent the transport of the fluid properties, such as momentum or temperature, across the fixed grid. If the planet was not rotating, the inertial motion of a parcel of gas would follow a great circle trajectory. In a spherical polar coordinate system, the great circle trajectory requires two extra terms in the momentum equation, which are shown later.

5. HORIZONTALLY STRATIFIED FLUID AND OTHER COMMON ASSUMPTION

One common assumption when addressing large-scale dynamics in atmospheric fluids is that the horizontal scale size is significantly greater than the vertical scale. This assumption implies that horizontal motions are constrained to follow the curvature of the planet. Another common assumption is that the vertical wind is significantly less than the horizontal wind, so the advection cross terms in the spherical polar coordinate system, $V_\theta V_z/r$ and $V_\phi V_z/r$, can be neglected. The shallow atmosphere approximation also enables several other assumptions: that gravity is independent of altitude and that the following terms can be neglected: vertical component and second-order terms of the Coriolis force, Earth's nonsphericity, centrifugal terms, and the increase in geocentric distance.

6. CORIOLIS EFFECT

Planetary rotation gives rise to the Coriolis force. The Coriolis effect is an apparent deflection of moving objects from a straight path when they are viewed from a rotating frame of reference. The apparent force is a consequence of the inertia of the fluid being constrained to move on a

horizontal curved surface. For planets with a rotational direction, the same as that of Earth's, a prograde rotation, the Coriolis effect away from the geographic equator causes a parcel of fluid moving with respect to the planetary rotation, to be directed toward the right in the Northern Hemisphere and to the left in the south. The basic force can be expressed as

$$-2\mathbf{\Omega} \times \mathbf{V} \tag{11}$$

where $\mathbf{\Omega}$ is the planet's angular velocity.

7. VISCOUS DRAG

Viscosity is the process that tends to smooth out gradients in the fluid and can be caused by molecular or turbulent diffusion. Strictly speaking, both processes smear out second-order gradients, $\partial^2/\partial z^2$. However, the imposed boundary condition at the top of the atmosphere that assumes that there is no mass flux through the upper boundary sets vertical gradients to zero and has the effect that viscosity acts to smear out first-order gradients, $\partial/\partial z$. In the upper thermosphere where diffusion is rapid, vertical viscosity is very effective in smoothing out the neutral wind and temperature profiles. Horizontal viscosity tends to have a weaker effect on the dynamics in global models due to the fact that horizontal spacing is large (200 to 500 km) compared to the vertical spacing (5 to 20 km). Note that horizontal viscosity is sometimes included in global models to assist with numerical stability.

8. ION DRAG

The basic processes driving the dynamics in an un-ionized fluid are advection, pressure gradients, Coriolis, and viscosity. In Earth's weakly ionized upper atmosphere, however, the presence of the intrinsic internal magnetic field gives rise to an additional force in the atmosphere known as ion drag. In the absence of electric fields and collisions with neutral particles, the ions are strongly constrained by the magnetic field. Plasma can flow freely parallel to the magnetic field direction, but flow perpendicular to the field is restricted.

In the upper thermosphere, the collision between the ions and neutral particles are relatively infrequent but are sufficient to cause a drag on the neutral flow. The basic force can be expressed as

$$-\nu_{ni}(\mathbf{V} - \mathbf{U}) \tag{12}$$

where the force is proportional to the difference in the neutral velocity, **V**, and the ion velocity, **U**, scaled by the neutral ion collision frequency, ν_{ni}. The simplicity of this formulism, however, hides a great deal of complexity in both the ion motion and the drag force as a function of altitude through the atmospheric domain. By adopting some reasonable assumptions, the ion drag force can also be written as $\mathbf{J} \times \mathbf{B}/\rho$ for a current, **J**, in the presence of a magnetic field, **B**.

9. MOMENTUM EQUATION

The momentum equations for the meridional and zonal direction for a unit mass of gas in the spherical polar coordinate system can therefore be stated thus

$$\frac{\partial}{\partial t}V_\theta = \underbrace{-\frac{V_\theta}{r}\frac{\partial}{\partial\theta}V_\theta - \frac{V_\phi}{r\sin\theta}\frac{\partial}{\partial\phi}V_\theta - \omega\frac{\partial}{\partial p}V_\theta}_{\text{horizontal and vertical advection}} \underbrace{-\frac{g}{r}\frac{\partial}{\partial\theta}h}_{\text{pressure}}$$
$$\underbrace{+\left(2\Omega + \frac{V_\phi}{r\sin\theta}\right)V_\phi\cos\theta}_{\text{Coriolis \& ``curvature''}} \underbrace{+ g\frac{\partial}{\partial p}\left[(\mu_m + \mu_T)\frac{p}{H}\frac{\partial}{\partial p}V_\theta\right]}_{\text{vertical viscosity}}$$
$$\underbrace{-\nu_{ni}(V_\theta - U_\theta)}_{\text{ion drag}} \tag{13}$$

and

$$\frac{\partial}{\partial t}V_\phi = -\frac{V_\theta}{r}\frac{\partial}{\partial\theta}V_\phi - \frac{V_\phi}{r\sin\theta}\frac{\partial}{\partial\phi}V_\phi - \omega\frac{\partial}{\partial p}V_\phi - \frac{g}{r\sin\theta}\frac{\partial}{\partial\phi}h$$
$$-\left(2\Omega + \frac{V_\phi}{r\sin\theta}\right)V_\theta\cos\theta + g\frac{\partial}{\partial p}\left[(\mu_m + \mu_T)\frac{p}{H}\frac{\partial}{\partial p}V_\phi\right]$$
$$-\nu_{ni}(V_\phi - U_\phi) \tag{14}$$

where V_θ and V_ϕ are the meridional and zonal neutral winds, and U_θ and U_ϕ are the meridional and zonal ion drifts, and the terms on the right are horizontal and vertical advection, horizontal pressure gradient, Coriolis and "curvature," vertical viscosity, and ion drag, respectively. The μ_m and μ_T expressions in the viscous drag term represent the molecular and turbulent viscous coefficients, respectively. Note that the terms mentioned previously that accommodate the inertial motion in the spherical polar coordinate system are included with the Coriolis term. These additional expressions are sometimes referred to as "curvature" terms. The momentum equations combined with the hydrostatic and continuity equations can be used to solve for the horizontal neutral wind across the globe. The vertical wind, ω, in the pressure coordinates is obtained by integrating the continuity equation from the top of the atmosphere down, where ω is set to zero at the top of the atmosphere, which assumes that there is no mass flux through the upper boundary.

10. ENERGY EQUATIONS

In a similar way, the energy equation can be stated thus

$$\frac{\partial}{\partial t}\varepsilon = \underbrace{-\frac{V_\theta}{r}\frac{\partial}{\partial\theta}(\varepsilon+gh)-\frac{V_\phi}{r\sin\theta}\frac{\partial}{\partial\phi}(\varepsilon+gh)-\omega\frac{\partial}{\partial p}(gh)}_{\text{advection and adiabatic processes}} + \underbrace{Q_{euv}}_{\text{sinks}} + \underbrace{Q_{ir}+Q_{vis}}_{\text{sinks}} + \underbrace{g\frac{\partial}{\partial p}\left[(\kappa_m+\kappa_T)\frac{p}{H}\frac{\partial}{\partial p}T\right]}_{\text{vertical heat conduction}} \underbrace{-g\frac{\partial}{\partial p}\frac{g\kappa_T}{c_p}}_{\text{kinetic energy dissipation}} - \underbrace{\frac{J_\theta E_\theta + J_\phi E_\phi}{\rho}}_{\text{Joule heating}} \quad (15)$$

where ε represents the sum of the specific enthalpy, or internal energy of the gas, c_pT, and the kinetic energy of a unit mass of gas, $(V_\theta^2 + V_\phi^2)/2$.

The terms on the right are horizontal and vertical advection of the sum of internal, kinetic, and potential energy; sources and sinks of energy such as solar EUV heating, IR cooling, and viscous heating; vertical heat conduction; and the sum of Joule heating and kinetic energy dissipation from ion drag, resulting from a current, **J**, and electric field, **E**. A parcel of gas that is displaced vertically by a turbulent eddy will undergo adiabatic heating or cooling, depending on whether the parcel has been displaced upward to a lower-pressure level where it will expand and cool or downward to a region of higher pressure where the gas will compress and heat. In the absence of local heat sources, the equilibrium vertical temperature profile under the action of turbulence is the adiabatic lapse rate, g/c_p. The extra conduction term, involving K_T, represents this process. In the region of molecular diffusion, individual atoms and molecules exchange locations, rather than parcels of gas, so the equilibrium temperature profile migrates toward isothermal.

Adiabatic processes cause changes in the temperature of a fluid in response to compression or expansion of a gas parcel. Solar heating initially imparts energy and provides the heat source for the upper atmosphere. Local or regional heating imposes horizontal pressure gradients that set the atmosphere in motion horizontally. The continuity of the global circulation is closed by upwelling in the region of divergence and downwelling in the region of convergence. Upwelling of a parcel of gas to a region of reduced pressure causes a parcel of gas to expand and adiabatically cool; downwelling transports parcels of air to regions of higher pressure causing compression and adiabatic heating. In the pressure coordinate system, the gas appears mathematically incompressible (see the continuity equation (8) above), so the physical concept of expansion and compression and adiabatic heating and cooling is represented by the term $\omega\partial gh/\partial p$ in equation (15).

As well as momentum transfer involved in the neutral/plasma interactions, there is also an energy exchange via the frictional dissipation from the movement of the ions through the neutrals or the neutrals through the ions. This frictional dissipation from the perspective of the neutral gas is known as Joule heating. This effect can also be described as the dissipation of a current flowing through the resistive medium of the neutral gas. The last term in equation (15), $(\mathbf{J}\cdot\mathbf{E})/\rho$, is the sum of Joule heating, $\mathbf{J}\cdot(\mathbf{E}+\mathbf{V}\times\mathbf{B})/\rho$, and kinetic energy dissipation from ion drag, $\mathbf{V}\cdot(\mathbf{J}\times\mathbf{B})/\rho$.

11. NEUTRAL COMPOSITION

Using a combination of the generalized diffusion equation [*Chapman and Cowling*, 1970] and the continuity equations, the change in composition of the three major thermospheric species (O, O_2, and N_2) can be evaluated self-consistently with the wind and temperature fields. The major species are atomic oxygen, molecular oxygen, and molecular nitrogen. Allowance is made for mutual molecular diffusion of the three species, horizontal and vertical advection, turbulent mixing vertically and horizontally, and production and loss mechanisms.

The continuity equation for mass mixing ratio, $\psi_i = n_i m_i/\rho$, of species, i, is given by

$$\underbrace{\frac{\partial\psi_i}{\partial t}}_{\substack{\text{rate of change}\\ \text{of mass mixing}\\ \text{ratio of species } i}} = \underbrace{\frac{1}{\rho}m_iS_i}_{\substack{\text{sources}\\ \text{and sinks}}} \underbrace{-\frac{V_\theta}{r}\frac{\partial}{\partial\theta}\psi_i - \frac{V_\phi}{r\sin\theta}\frac{\partial}{\partial\phi}\psi_i}_{\text{horizontal advection}} \underbrace{-\omega\frac{\partial}{\partial p}\psi_i}_{\text{vertical advection}} \underbrace{-\frac{1}{\rho}\nabla\cdot(n_im_i\mathbf{C}_i)}_{\text{molecular diffusion}} + \underbrace{\frac{1}{\rho}\frac{\partial}{\partial p}\left(K_T\frac{\partial}{\partial p}m\psi_i\right)}_{\text{eddy diffusion}} \quad (16)$$

where m_i is its molecular mass, S_i represents sources and sinks of the species, n_i, its number density, and C_i are the relative diffusion velocities. The terms on the right-hand side of the continuity equation for the species are, in their respective order, chemical sources and sinks of the species, horizontal meridional and zonal advection, vertical advection, mutual molecular diffusion between species, and eddy diffusion.

The molecular diffusion velocities are evaluated from the general diffusion equation for a multispecies gas given by

$$\frac{1}{n}\sum_{j\neq i}\left(\frac{\psi_i}{m_j D_{ij}} n_j m_j C_j - \frac{\psi_j}{m_j D_{ij}} n_i m_i C_i\right) = \nabla\psi_i + \frac{\psi_i}{m}\nabla m + \left(1-\frac{m_i}{m}\right)\frac{\psi_i}{mp}\nabla p \qquad (17)$$

where D_{ij} is the mutual diffusion coefficient between species i and j, and m is the mean molecular mass of the gas. For Earth's thermosphere, consisting of O, O_2, and N_2, equation (17) is a system of three coupled equations for the three major constituents, $i = 1$, 2, and 3.

In the lower atmosphere of planets, the fluid is very well mixed, and the mean molecular mass of the fluid is constant. For instance, the relative proportion of molecular nitrogen and molecular oxygen in the atmosphere is remarkably consistent from the surface to about 110 km altitude. The altitude where mixing gives way to molecular diffusion is known as the homopause or turbopause. Below this level, the air is constantly being mixed by turbulent wave eddies. In large-scale or global physics-based models, this process is usually parameterized as an eddy diffusion coefficient, K_T, (see equation (16)). Above about 110 km, turbulent mixing gives way to molecular mixing processes, and each species begins to be distributed vertically under its own pressure scale height or hydrostatic balance (see equation (4)). A heavy species, such as carbon dioxide, will decrease in concentration with height more rapidly than a light species such as atomic oxygen. Each species will have its own characteristic scale height, $RT/m_i g$, which is the vertical distance a species will decrease in number density by a fraction of $1/e$. Thus, above the homopause, the mean mass of the fluid will change with altitude, as well as other gas parameters such as the specific heat, c_p.

The vertical distribution of species is therefore affected by the balance between turbulent mixing and diffusive separation. Traditionally, the point of transition where both processes contribute equally has been termed the turbopause, which is typically assigned to an altitude of about 110 km for Earth's atmosphere. This altitude, of course, can vary with location and season depending on the strength of the gravity waves and other sources from the lower atmosphere responsible for the mixing and the likelihood the waves will break. The process of gravity wave breaking is a complex field and will not be discussed further.

The global seasonal/latitudinal structure of composition is also affected by a physical process called wind-induced diffusion [*Mayr et al.*, 1978]. This is somewhat of a misnomer because the process is actually advection or the simple transport of species. During solstice, the warmer summer hemisphere and colder winter hemisphere introduces a pressure gradient force in the direction from the summer to winter hemisphere. In the absence of drag, zonal winds would develop such that the Coriolis force from the zonal winds would balance the meridional pressure gradient, a condition known as geostrophic balance. In reality, the zonal winds experience drag from collisions with ions or from viscosity so that this pure geostrophic balance rarely occurs. The imbalance result is an interhemispheric circulation from summer to winter. Closure of this circulation drives an upwelling of material across pressure surfaces in the summer hemisphere and a downwelling in the winter hemisphere. The upwelling causes the heavier molecular-rich gas, which had diffusively separated out at lower altitudes, to be transported upward to increase the mean molecular mass in summer. In winter, the downwelling reduces the mean mass.

The large-scale global seasonal circulation is analogous to a huge interhemispheric mixing cell, or "thermospheric spoon," a global equivalent of the small-scale turbulent mixing cells in the lower atmosphere [*Fuller-Rowell*, 1998]. The implication is that the upper atmosphere is better mixed at solstice. Through the Earth year, there will be peaks in mixing in June and December. At equinox, the weaker global circulation allows the atmosphere to separate out more by molecular diffusion. The difference is subtle, but there are several consequences of this semiannual variation.

First, the globally averaged mean mass will vary semiannually. Second, since the scale height, or thickness of the upper atmosphere, depends on the mean molecular mass, the atmosphere will be more compressed at solstice and more expanded at equinox. This semiannual breathing of the upper atmosphere introduces a semiannual variation in neutral density. Third, since the production and loss rate of the ionosphere is dependent on neutral composition, a semiannual variation in plasma density is introduced. The "thermospheric spoon" does not appear to generate all of the observed magnitude of the semiannual variation. Additional processes from lower atmosphere mixing, and changes in eddy diffusion, are also operating [*Qian et al.*, 2009].

The relatively simple pattern of summer-to-winter circulation is augmented by the addition of the high-latitude magnetospheric, or "geomagnetic," sources. These heat sources tend to reinforce the solar radiation-driven equatorward flow in the summer hemisphere and compete with the poleward flow in winter. During geomagnetic storms, the high-latitude source can dominate the solar-driven circulation.

12. GLOBAL WIND, TEMPERATURE, DENSITY, AND COMPOSITION STRUCTURE

The basic momentum and energy equations and physical processes are captured in the thermospheric components of

the Coupled Thermosphere Ionosphere Model (CTIM) and Coupled Thermosphere Ionosphere Plasmasphere electrodynamics (CTIPe) models [*Fuller-Rowell and Rees*, 1980, 1983; *Fuller-Rowell et al.*, 1987, 1996a] and the Thermosphere General Circulation Model (TGCM), Thermosphere Ionosphere General Circulation Model (TIGCM), and Thermosphere Ionosphere Electrodynamics General Circulation Model (TIEGCM) suite of NCAR models [*Dickinson et al.*, 1981, 1984; *Roble et al.*, 1982, 1987, 1988]. An example of the global distribution of temperature and horizontal winds, at a fixed pressure level near 300 km altitude is shown in the top panels of Figure 1. The conditions are December solstice at fairly high solar activity and moderate geomagnetic activity. On the top left are contours of temperature with winds as vectors, and on the top right are contours of the meridional wind. December solstice conditions render the Southern Summer Hemisphere hotter, and Earth's rotation introduces a significant diurnal or day/night temperature and meridional wind difference. The winds at high latitude are the largest because a modest magnetospheric convection electric field has been imposed to drive the ions, which subsequently accelerate the neutrals through ion drag (see term in equations (13) and (14)). The solar-driven winds tend to blow away from the high-pressure area under the subsolar point to the low-pressure area at the antipodal solar point on the nightside. Thus, daytime meridional winds tend to be poleward, while nighttime meridional winds tend to be equatorward and larger partly because of the lower ion drag on the nightside.

The left lower panel of Figure 1 shows the neutral density at a fixed height of 300 km. The same seasonal latitude structure is apparent with higher densities in the summer hemisphere and with a large diurnal variation at mid and low latitudes. The lowest density and temperature is near the antipodal solar point on the nightside. The right lower panel of Figure 1 shows the ratio of the height-integrated atomic oxygen to molecular nitrogen O/N_2. The upwelling in the Southern Summer Hemisphere raises the concentration of the heavier molecular species giving the smaller O/N_2 and larger mean mass compared with the downwelling and increases in O/N_2 or decreases in the mean mass in the winter hemisphere. Since, as described above, the heating and cooling itself does not directly change the O/N_2 ratio, the composition distribution is somewhat different from the temperature and density. The main feature is summer-to-winter circulation creating the seasonal/latitude structure. The peak in the winter hemisphere is displaced to mid latitudes by the high-latitude Joule heating. A secondary feature is the weaker diurnal variation. The mixing of neutral composition by the global circulation impacts the ionosphere. Ion loss rates are faster in the molecular-rich atmosphere so the neutral composition structure gives rise to a seasonal ionospheric anomaly, where dayside winter plasma densities are greater than in winter.

The equations of momentum and energy described above can also support the propagation of large-scale gravity waves. Figure 2 shows a snapshot of the change in neutral wind at mid and low latitudes at 250 km at the December solstice 3 h into a numerical simulation of a step-function increase in high-latitude forcing in the auroral oval (65° to 75° geomagnetic latitude). The wind response is shown within 50° latitude of the geographic equator, to allow for a scale that clearly shows the mid- and low-latitude dynamic response. Whereas at auroral latitudes, the peak neutral winds would be several hundred m s^{-1}, at mid and low latitudes, the wind surges are typically100 to 200 m s^{-1} above the background circulation. At this time, 3 h into the simulation, the disturbance winds have reached the equator and are beginning to penetrate the other hemisphere and interact with the opposing wavefront from the other pole. The arrival of the wavefront at the geographic equator within 3 h indicates a propagation speed of about 700 m s^{-1}, in this case. This speed is consistent with observations of traveling ionosphere disturbances (TIDs). A vertical cut through the thermosphere would reveal a tilted wave front with the wave propagating more slowly at the lower altitudes [*Richmond and Matsushita*, 1975].

Observations and model simulations reveal a "sloshing" of winds between hemispheres in response to the high-latitude heating during a storm. The net integrated wind effect is for an increase in the global circulation from pole to equator in both hemispheres [*Roble*, 1977; *Forbes*, 2007]. The change in circulation transports all neutral parameters including temperature, density, and species composition. The neutral composition changes and their impact on the ionosphere are dealt with below.

13. THERMAL EXPANSION

There are several misconceptions regarding temperature changes and changes in neutral composition. Heating the atmosphere locally and the resultant thermal expansion does not change the ratio of neutral species (e.g., O/N_2) on pressure surfaces, but it does change on height levels. Since the pressure levels are levels of constant optical depth, ionization rates from solar photons or auroral particles do not change as a result of the heating because the photons or particles have to penetrate the same amount of atmosphere. So to first order, neither the ion production nor loss rates change on the pressure surface. "Real" changes in neutral composition on a pressure surface are caused by the upwelling through the pressure surfaces by the global circulation.

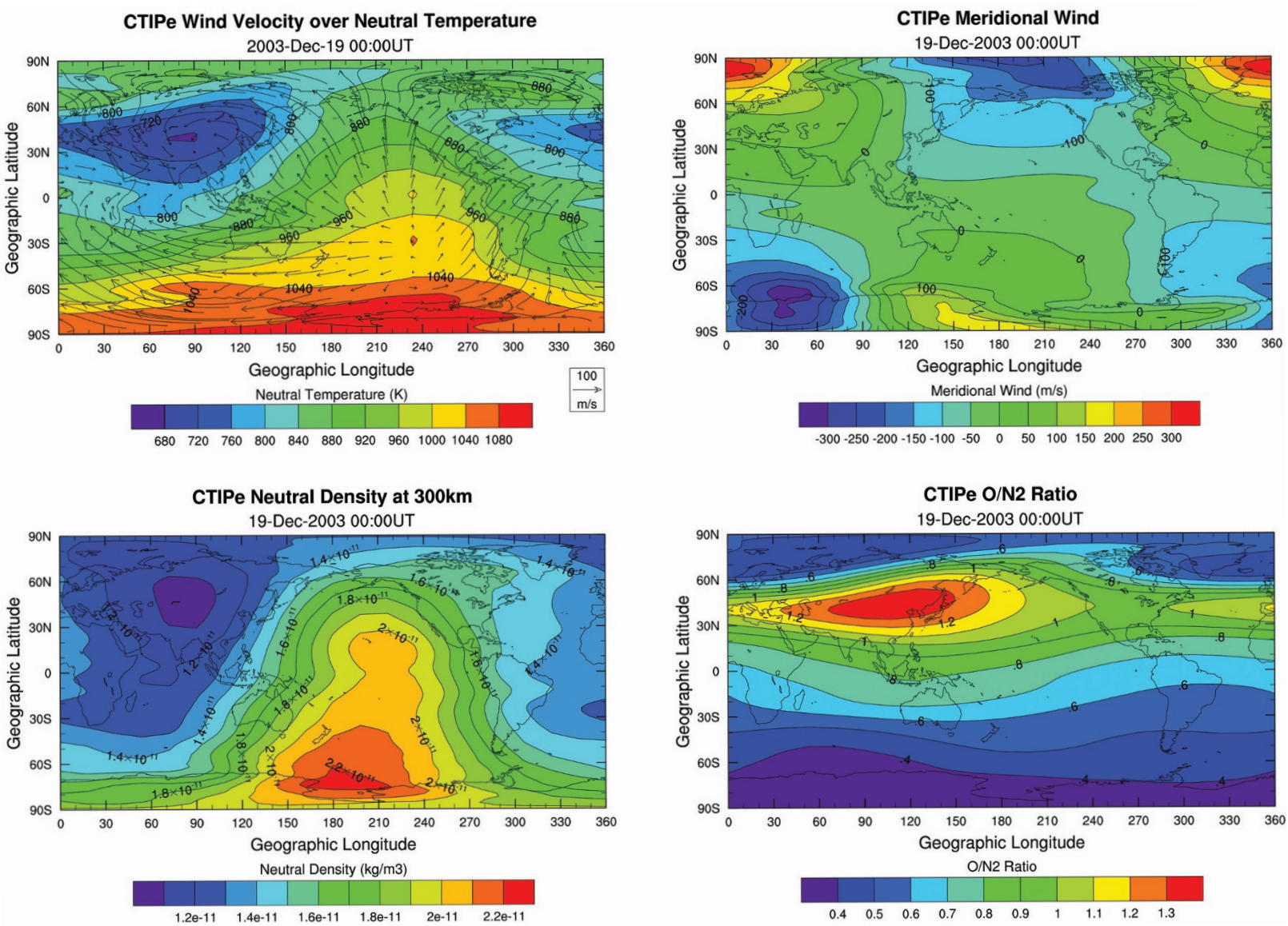

Figure 1. Typical global distribution of some of the major model parameters at the December solstice at moderate solar and geomagnetic activity. (left top) The contours of neutral temperature and total wind vector and (right top) the contours of meridional wind on a fixed pressure level in the upper thermosphere close to 300 km. (left bottom) Neutral density at a fixed altitude of 300 km and (right bottom) the height-integrated O/N_2 ratio (figure courtesy of *Mariangel Fedrizzi*, 2012).